



# The State and the Variations of Greenhouse Gases in the Atmosphere

*The content of this communication is based on the information that is included in the annual WMO Greenhouse Gas Bulletins produced during the last 14 years on the basis of the long-term high-quality observations undertaken by the global network and taking into consideration the recent advances in greenhouse gas research. The information is prepared by the Scientific Advisory Group on Greenhouse Gases under the Global Atmosphere Watch (GAW) Programme of WMO.*

## 1. Current levels of Greenhouse Gases in the atmosphere and trends

### 1.1 Globally averaged levels in 2018 and 2017

The latest analysis of observations from the GAW Programme shows that globally averaged surface mole fractions (the quantity representing concentration) calculated from this in situ network

for carbon dioxide (CO<sub>2</sub>), methane (CH<sub>4</sub>) and nitrous oxide (N<sub>2</sub>O) reached new highs in the past years. In 2018, the global averaged CO<sub>2</sub> mole fraction was 407.8±0.1 ppm, 2.2 ppm higher than in 2017. Preliminary data from a subset of greenhouse gas (GHG) observational sites for 2019 indicate that CO<sub>2</sub> concentrations are on track to reach or even exceed 410 ppm by the end of 2019.

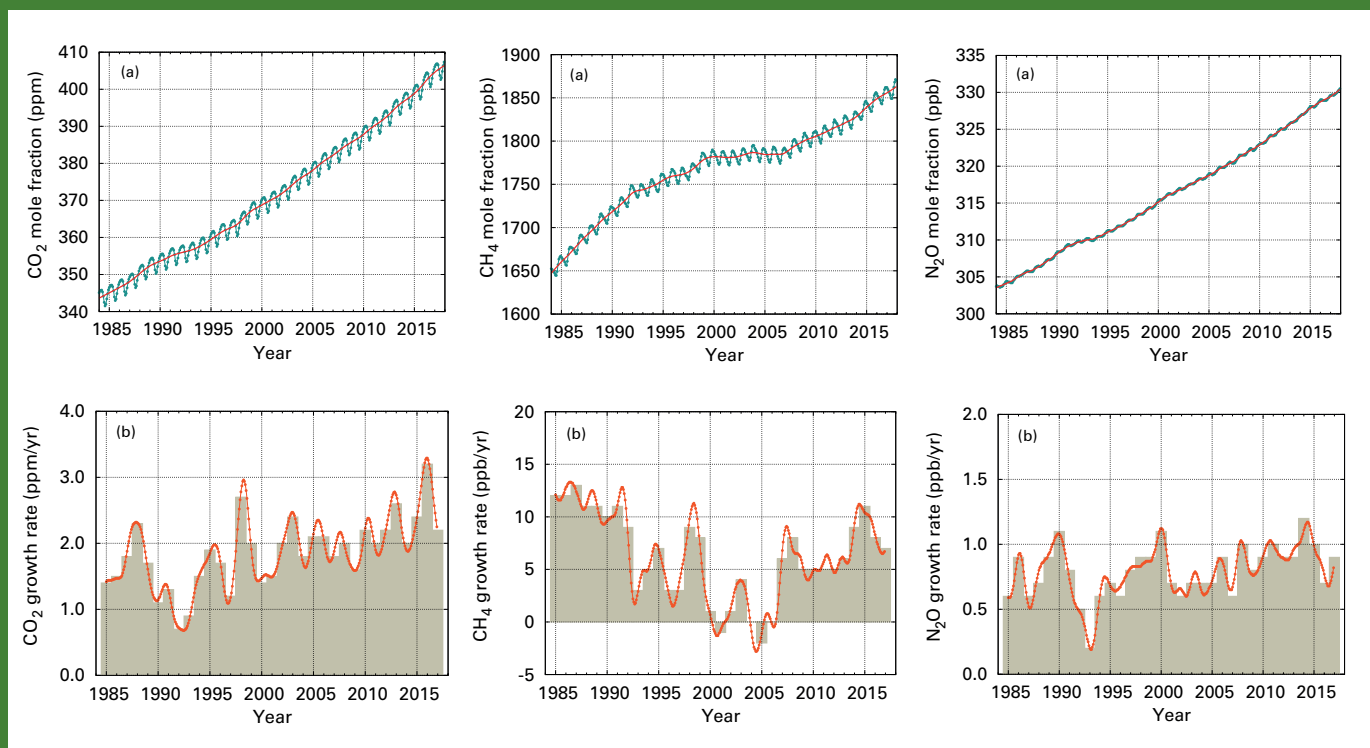


Figure 1. Evolution of the global averaged mole fractions for the major greenhouse gases CO<sub>2</sub>, CH<sub>4</sub> and N<sub>2</sub>O from 1985 until 2018, based on the WMO GAW in situ network observations. The red line depicts the de-seasonalized trend. The bottom plots show the respective monthly growth rates derived from the evolution of the global averages for each of the gases over the period.

A full global analysis completed for the three main greenhouse gases shows that in 2017, globally averaged mole fractions of CO<sub>2</sub> were 405.6 ±0.1 ppm, CH<sub>4</sub> at 1859 ±2 ppb and N<sub>2</sub>O at 329.9 ±0.1 ppb. These values constitute, respectively, 146%, 257% and 122% of pre-industrial levels (pre-1750).

The increase in CO<sub>2</sub> from 2017 to 2018 was equal to that from 2016 to 2017 but smaller than that observed from 2015 to 2016. This annual increase is practically equal to the average growth rate over the last decade. The influence of the El Niño event that peaked in 2015–2016 and contributed to the increased growth rate in 2015–2016, has sharply declined in the years 2017 and 2018. The growth rate of CO<sub>2</sub> averaged over three consecutive decades (1985–1995, 1995–2005 and 2005–2015) increased from 1.42 ppm/y to 1.86 ppm/y and to 2.06 ppm/y with the highest annual growth rates observed during El Niño events.

For CH<sub>4</sub>, the increase from 2016 to 2017 is lower than that observed from 2015 to 2016 but practically equal to the average over the last decade. For N<sub>2</sub>O, the increase from 2016 to 2017 was higher than that observed from 2015 to 2016 and practically equal to the average growth rate over the past 10 years. Figure 1 shows the evolution of the global mean values derived from the WMO GAW global network of observations for the major greenhouse gases.

*There is to this date no sign of the peaking of the global greenhouse gas levels and CO<sub>2</sub> continues to increase at the record growth rates during the last decade.*

## 1.2 The global network

The GAW Programme (<http://www.wmo.int/gaw>) coordinates systematic observations and analysis of greenhouse gases and other trace species. Sites where greenhouse gases have been measured in the last decade are shown in Figure 2. The GAW greenhouse gas network has been designed to measure the atmospheric content very accurately, with so called compatibility goals for CO<sub>2</sub> of 0.1 ppm (at a value of about 400 ppm this is 0.02% accuracy and precision) and 1 ppb for CH<sub>4</sub> (at 1850 ppb this is 0.05% accuracy and precision). That means that any value measured at a GAW station can be compared with any other station within that uncertainty. The greenhouse gas community undertakes efforts to review the measurement techniques and the global requirements for the quality of measurements and harmonized protocols at the biannual meetings of expert taking place since 1975 and co-organized by the International Atomic Energy Agency since 1997.

Measurement data are reported by participating countries and archived and distributed by the World Data Centre for Greenhouse Gases (WDCGG)

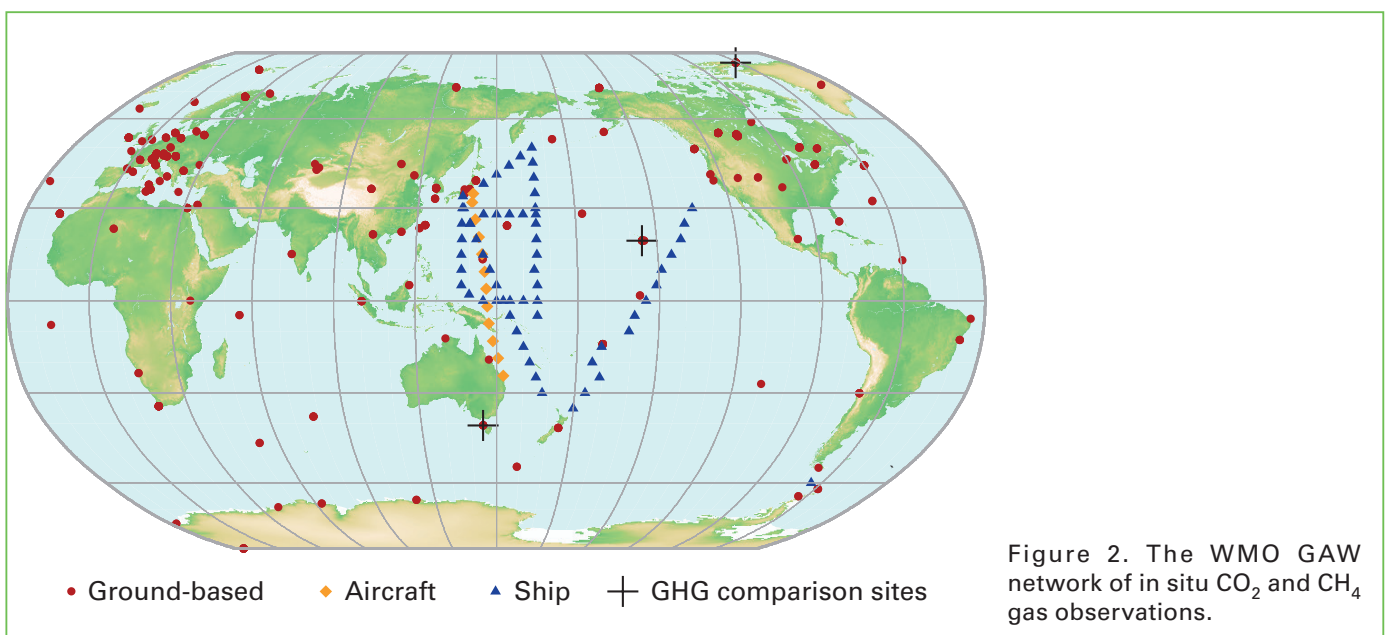
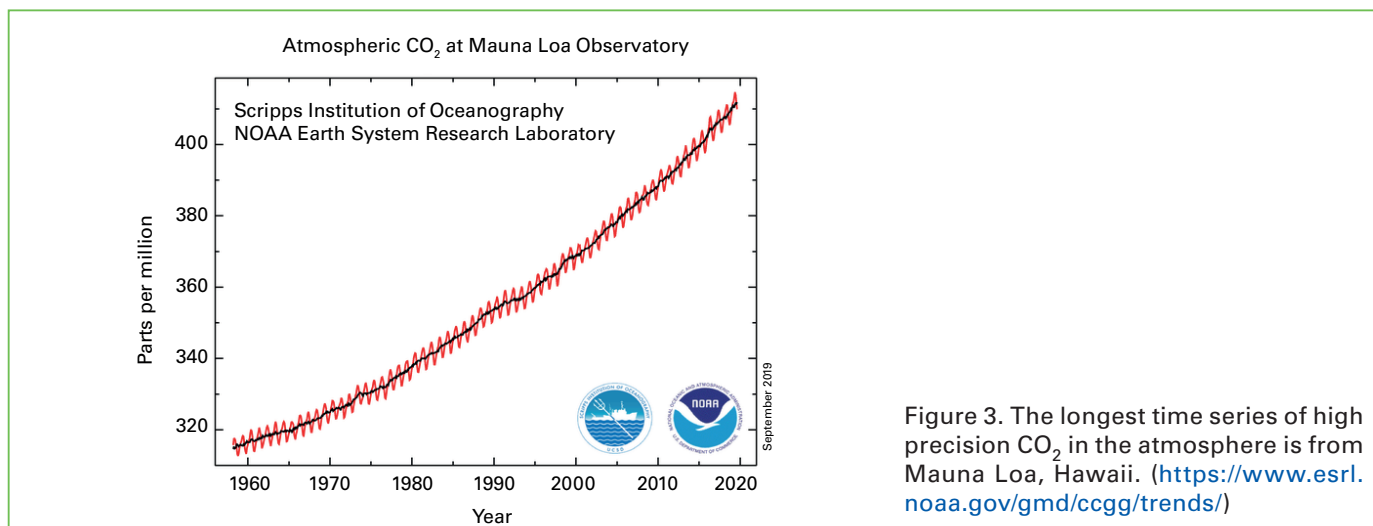


Figure 2. The WMO GAW network of in situ CO<sub>2</sub> and CH<sub>4</sub> gas observations.



at the Japan Meteorological Agency. The data are available free of charge for interested audience.

### 1.3 Initiation of the greenhouse gas measurements

Measurements of atmospheric CO<sub>2</sub> can provide strong insights into human induced variations in the global carbon cycle. The rise in atmospheric CO<sub>2</sub> has been well documented since 1958, when high precision measurements began at Mauna Loa, under the direction of C. D. Keeling, as shown in Figure 3. The practices applied then to ensure high-quality measurements were adopted for the observations by GAW participants and are currently applied at over one hundred stations worldwide.

Figure 3 represents the so called “Keeling curve” and shows the monthly mean CO<sub>2</sub> mole fractions measured at Mauna Loa Observatory, Hawaii. The National Ocean and Atmospheric Administration (NOAA) started its own CO<sub>2</sub> measurements in May 1974, and they have run in parallel with those made by the Scripps institute since then. The Mauna Loa data are being obtained at an altitude of 3400 m in the northern subtropics and are very similar to but different from the globally averaged CO<sub>2</sub> concentration at the surface due to the global mixing and smoothing of the signals (see section 2.2). Preliminary analysis shows that CO<sub>2</sub> annual mean mole fraction at Mauna Loa in 2018 reached 408.52 ppm (in comparison with 407.8 ppm globally averaged) and the increase from 2017 to 2018 was 1.97 ppm. From January 2019 to August 2019 the increase in the mole fraction (de-seasonalized trend) was 0.85ppm.

## 2. Variability of greenhouse gas levels

### 2.1 Spatial and temporal variations in the greenhouse gas levels

There is substantial variability in the levels of greenhouse gases within individual years (seasonal cycle), between years and between different geographic regions. An example of the temporal-spatial variability of CO<sub>2</sub> is presented in Figure 4. The variability of CO<sub>2</sub> in the Northern Hemisphere is larger than in the Southern Hemisphere. The seasonal cycles (the wiggles within one year in Figure 4) are clearly larger in amplitude in northern high and mid-latitudes and small in the Southern Hemisphere. The seasonal cycle in the Northern Hemisphere is mainly dominated by the land biosphere, and it is characterized by rapid decreases with 5–20 ppm from June to August and large returns of similar magnitude from September to December. Large-scale spatial gradient exists for the other greenhouse gases as well.

### 2.2 Variability of the greenhouse gas levels at the individual stations

All GAW stations show the same global increases, mixed with more local influences depending on the station location and height. These local influences can be used to study the local and/or regional sources and sinks of the greenhouse gases. These signals help to reduce uncertainties of our emission estimates or warn for emissions signals from unknown sources or previously

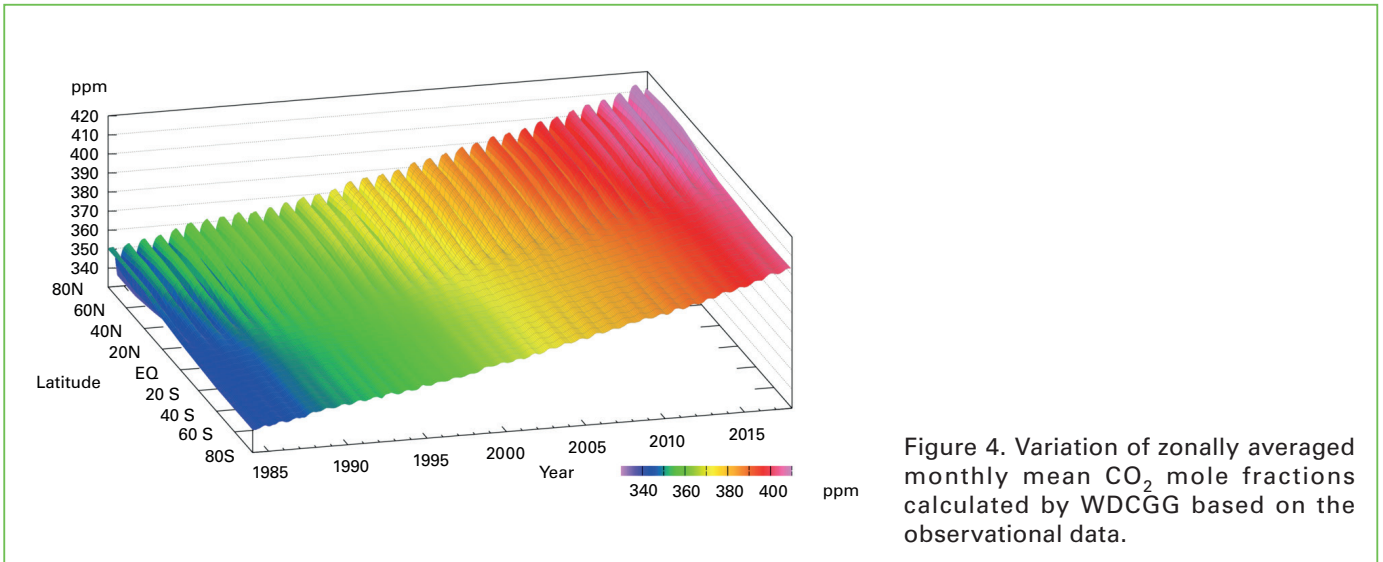


Figure 4. Variation of zonally averaged monthly mean CO<sub>2</sub> mole fractions calculated by WDCGG based on the observational data.

not captured processes under the influence of ongoing climate change that feedback into the greenhouse gas emissions, e.g. droughts, floods, land use changes and permafrost melting.

Figure 5 demonstrates the CO<sub>2</sub> atmospheric signal captured at three stations in Japan over the period 1987 until now, showing similar signals as Mauna Loa but mixed with local variability. The signal from all stations captures the global increase very well with differences that inform us on the more local sources and sinks. One can also see that the monthly mean levels of CO<sub>2</sub> with the removed seasonal cycle already exceed 410 ppm in 2019 at these sites.

Another illustration is shown in Figure 6 through the atmospheric signal captured at high

latitude in Europe at Pallas station (part of GAW contributing network ICOS) in northern Finland. This station, like now many of the GAW stations, has continuous measurements at high temporal hourly resolution, which delivers more information than the traditional weekly or bi-weekly flask measurements. The black dots here identify the hourly observations that show even more variability, linked to signals from the natural carbon cycle and anthropogenic emissions. The blue line is derived from the hourly data by a seasonal statistical fit. The same fit for Mauna Loa is shown here as the red curve. Clearly, both Mauna Loa and Pallas show the same global increase in annual concentration, but the Pallas data show a larger seasonal variation due to larger activity of the biosphere around the position of the station and its latitude, where Mauna Loa as bare

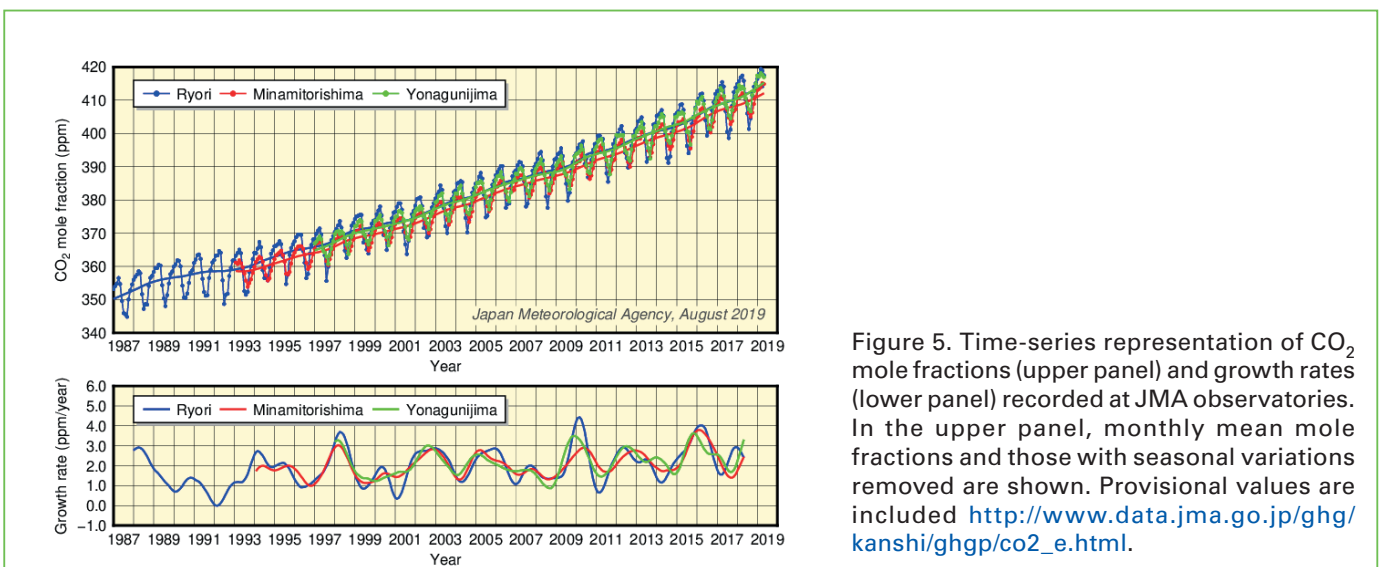


Figure 5. Time-series representation of CO<sub>2</sub> mole fractions (upper panel) and growth rates (lower panel) recorded at JMA observatories. In the upper panel, monthly mean mole fractions and those with seasonal variations removed are shown. Provisional values are included [http://www.data.jma.go.jp/ghg/kanshi/ghgp/co2\\_e.html](http://www.data.jma.go.jp/ghg/kanshi/ghgp/co2_e.html).

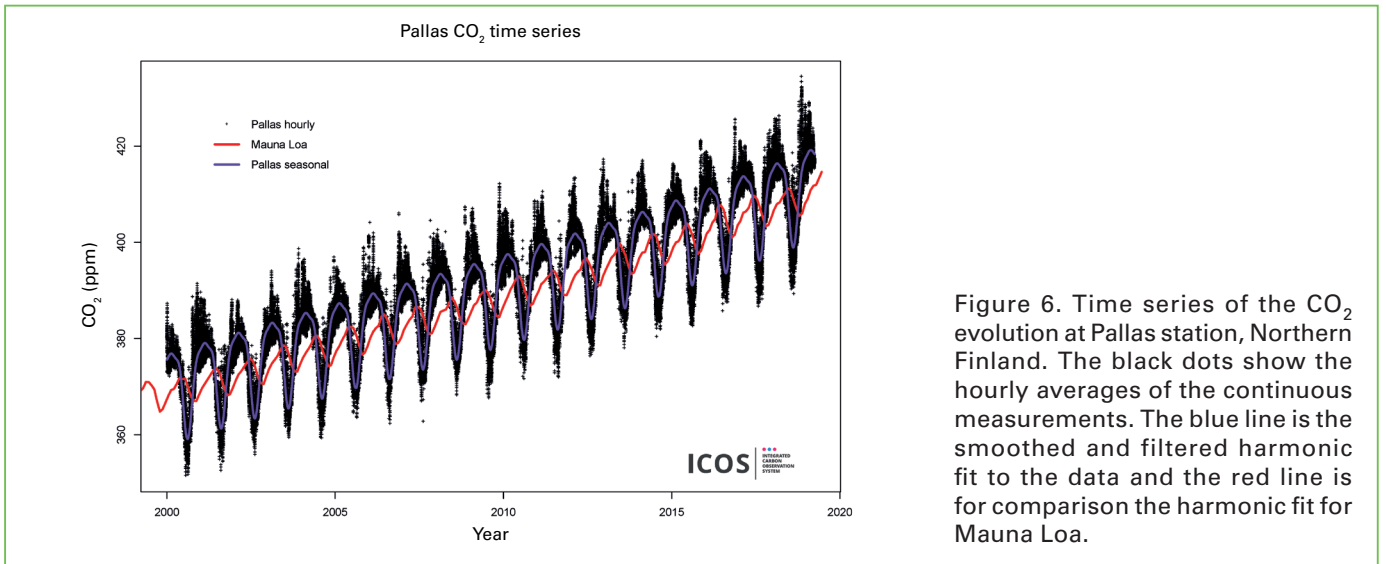


Figure 6. Time series of the CO<sub>2</sub> evolution at Pallas station, Northern Finland. The black dots show the hourly averages of the continuous measurements. The blue line is the smoothed and filtered harmonic fit to the data and the red line is for comparison the harmonic fit for Mauna Loa.

mountain top has no nearby biospheric activity. Please note that at Pallas station the 410 ppm CO<sub>2</sub> was already reached in winter 2013 and wintertime CO<sub>2</sub> in 2019 already exceeded 430 ppm. The CO<sub>2</sub> variations at the hourly timescale are representative for a region around the tower of roughly 500–1000 km distance, but this can vary depending on many factors.

The levels of CO<sub>2</sub> in the Southern Hemisphere are less variable and lower than the global averages as presented in Figure 7. Atmospheric CO<sub>2</sub> is measured continuously at Baring Head, New Zealand, providing the longest running record of this type in the southern hemisphere. Observations at this station were started in the early 1970s and continue to the present.

Preliminary analysis shows that CO<sub>2</sub> annual mean mole fraction at Baring Head in 2018 reached 404.78 ppm and the increase from 2017 to 2018 was 2.5 ppm. From January 2019 to August 2019, the increase in the mole fraction (de-seasonalized trend) was 1.51 ppm.

### 2.3 Sources and sinks of greenhouse gases

The accumulated amount of the greenhouse gases in the atmosphere is a result of the budget between emissions from sources and uptakes by sinks. The Global Carbon Project (GCP) performs yearly analyses of the accumulation of CO<sub>2</sub> in the atmosphere and the budget of the contributions of sources and sinks. [Further details can be found in the GCP contribution.](#)

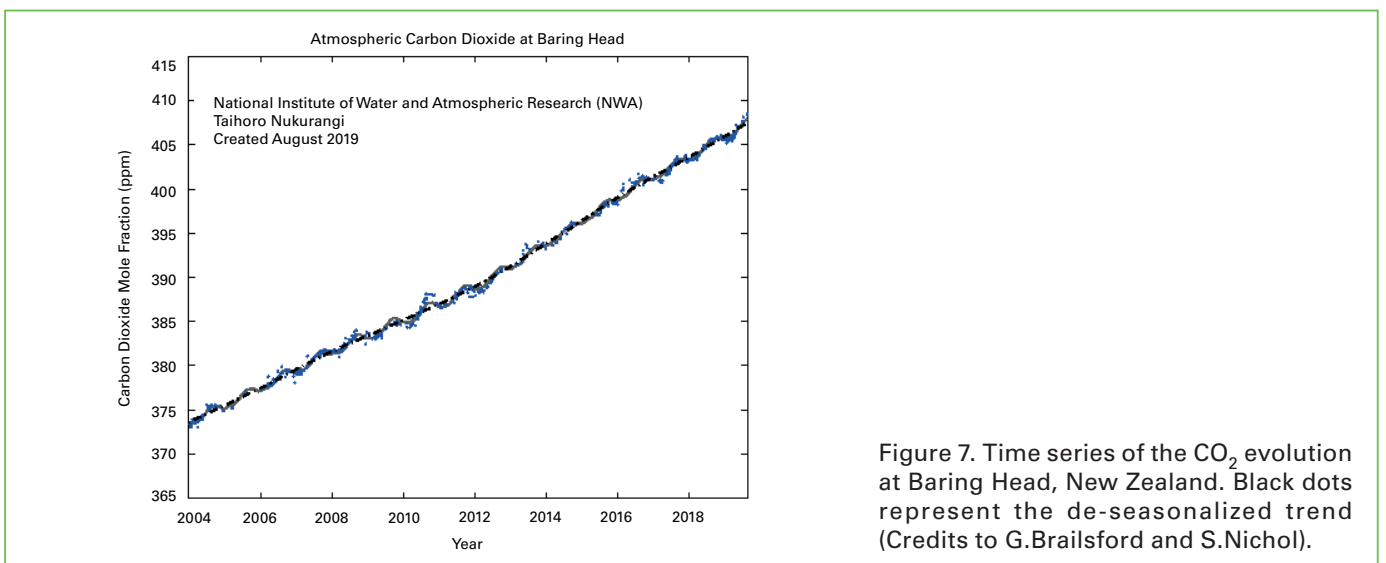


Figure 7. Time series of the CO<sub>2</sub> evolution at Baring Head, New Zealand. Black dots represent the de-seasonalized trend (Credits to G.Brailsford and S.Nichol).

Carbon dioxide is the single most important anthropogenic greenhouse gas in the atmosphere, contributing ~65.8% of the radiative forcing by long lived greenhouse gases (LLGHGs). It is responsible for ~82% of the increase in radiative forcing over the past decade and over the past five years. The pre-industrial level of 278 ppm represented a balance of fluxes among the atmosphere, the oceans and the land biosphere. Atmospheric CO<sub>2</sub> reached 146% of the pre-industrial level in 2017, primarily because of emissions from combustion of fossil fuels and cement production (the sum of CO<sub>2</sub> emissions was 9.9±0.5 PgC in 2016), deforestation and other land-use change (1.3±0.7 PgC average for 2007–2016), as reported by GCP. Of the total emissions from human activities during the period 2007–2016, about 44% accumulated in the atmosphere, 22% in the ocean and 28% on land, the unattributed budget imbalance is 5%.

Methane contributes ~17% of the radiative forcing by LLGHGs. Approximately 40% of methane is emitted into the atmosphere by natural sources (e.g., wetlands and termites), and about 60% comes from anthropogenic sources (e.g., ruminants, rice agriculture, fossil fuel exploitation, landfills and biomass burning). Atmospheric CH<sub>4</sub> reached 257% of the pre-industrial level (~722 ppb) due to increased emissions from anthropogenic sources.

Nitrous oxide contributes ~6% of the radiative forcing by LLGHGs. It is the third most important

individual contributor to the combined forcing. N<sub>2</sub>O is emitted into the atmosphere from both natural (about 60%) and anthropogenic sources (approximately 40%), which include oceans, soils, biomass burning, fertilizer use, and various industrial processes. The globally averaged N<sub>2</sub>O mole fraction in 2017 reached 122% of the pre-industrial level (270 ppb).

Atmospheric observations of the isotopic composition of GHG and/or of the related tracers provide some insights into the magnitude of the sources and sinks of GHGs. The rise of CO<sub>2</sub> concentration is currently only about half of what would be expected if all the excess CO<sub>2</sub> from burning of fossil-fuels and land use changes would have stayed in the air. The other half has been absorbed by the land biosphere and the oceans, but the split between land and oceans is not easily resolved from CO<sub>2</sub> data alone. Here is where oxygen (O<sub>2</sub>) measurements prove to be useful.

One of the longest O<sub>2</sub> time series, from flasks collected at Cape Grim, Tasmania and analyzed at the Scripps Institution of Oceanography is shown on the right in Figure 8. O<sub>2</sub> abundance is reported as relative changes in the O<sub>2</sub>/N<sub>2</sub> ratio. A decrease of 100 per meg corresponds to the loss of 100 O<sub>2</sub> molecules for every million O<sub>2</sub> molecules in the atmosphere. Atmospheric O<sub>2</sub> has decreased very slightly as it is consumed during the combustion of fossil fuels. The observed decrease in O<sub>2</sub>

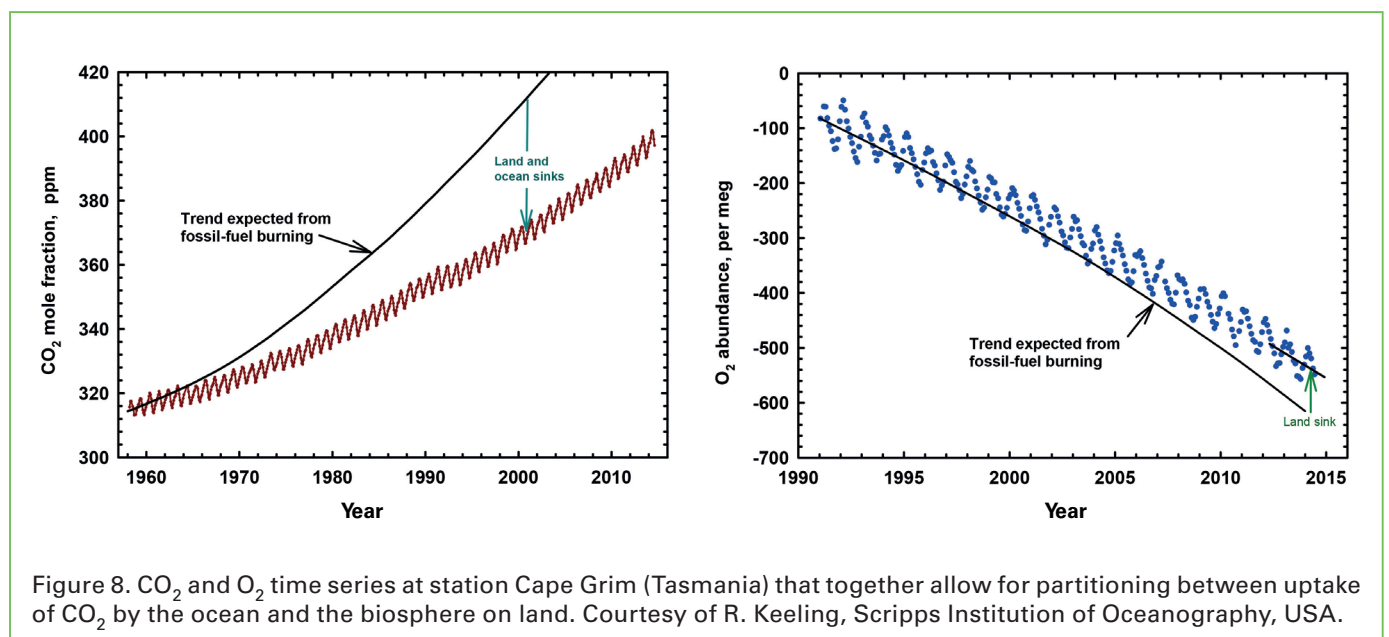


Figure 8. CO<sub>2</sub> and O<sub>2</sub> time series at station Cape Grim (Tasmania) that together allow for partitioning between uptake of CO<sub>2</sub> by the ocean and the biosphere on land. Courtesy of R. Keeling, Scripps Institution of Oceanography, USA.

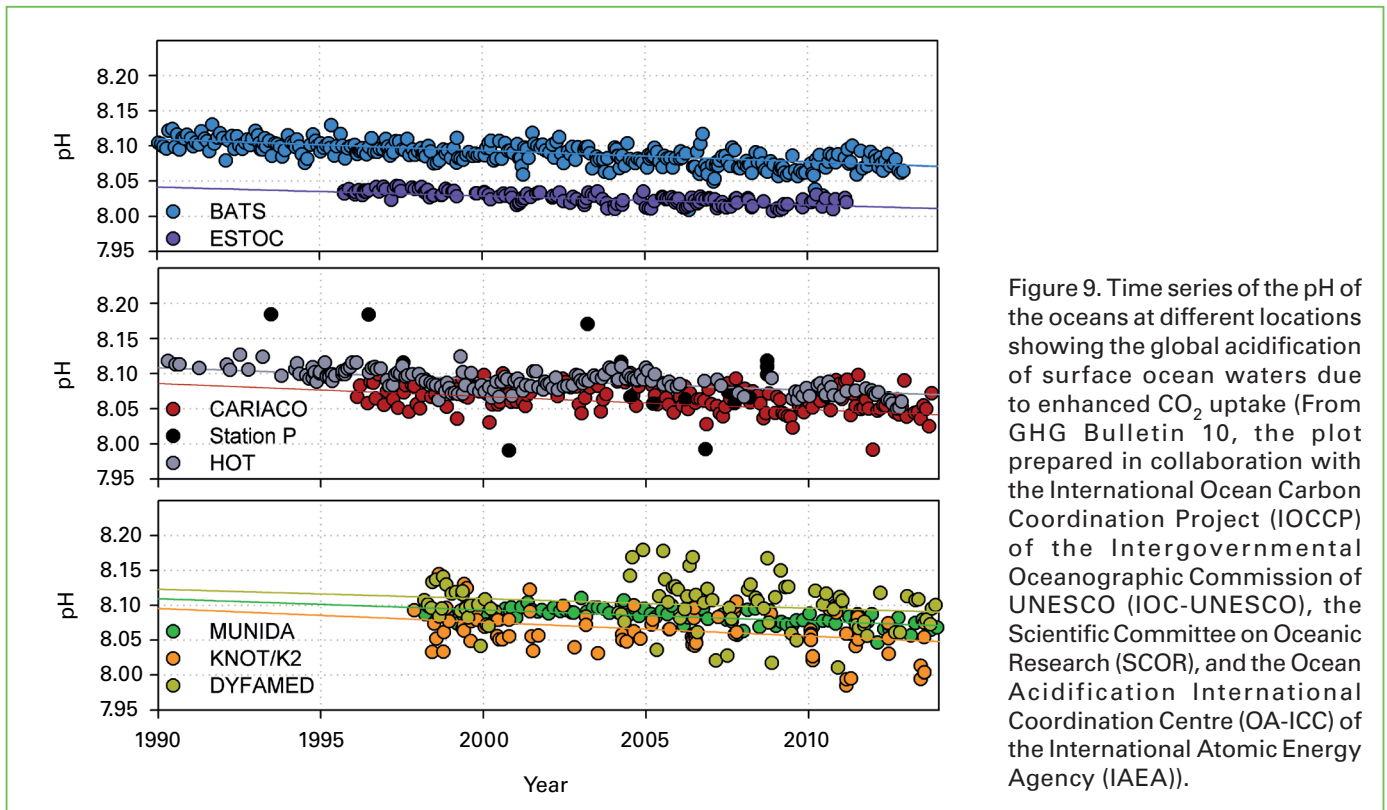


Figure 9. Time series of the pH of the oceans at different locations showing the global acidification of surface ocean waters due to enhanced  $\text{CO}_2$  uptake (From GHG Bulletin 10, the plot prepared in collaboration with the International Ocean Carbon Coordination Project (IOCCP) of the Intergovernmental Oceanographic Commission of UNESCO (IOC-UNESCO), the Scientific Committee on Oceanic Research (SCOR), and the Ocean Acidification International Coordination Centre (OA-ICC) of the International Atomic Energy Agency (IAEA)).

is less than predicted by the amount of fossil fuels combusted, because, as plants take up  $\text{CO}_2$  through photosynthesis, by which process  $\text{O}_2$  is returned to the atmosphere. The  $\text{O}_2$  offset therefore quantifies the magnitude of the land  $\text{CO}_2$  sink. The ocean  $\text{CO}_2$  sink can then also be calculated based on the requirement that the combined sinks sum to the total, established from the  $\text{CO}_2$  data. The  $\text{O}_2$  data also resolve fluctuations seasonally and on other time scales, which provide additional information about the large-scale functioning of the Earth's biosphere that complement  $\text{CO}_2$  data.

The ocean currently absorbs about one fourth (amounting to about 1500 kg  $\text{CO}_2$  per year per person) of the anthropogenic  $\text{CO}_2$  emissions, reducing the increase in atmospheric  $\text{CO}_2$  that would otherwise occur because of fossil fuel combustion. Enhanced ocean  $\text{CO}_2$  uptake alters the marine carbonate system that controls seawater acidity. As  $\text{CO}_2$  dissolves in seawater it forms carbonic acid ( $\text{H}_2\text{CO}_3$ ), a weak acid that dissociates into bicarbonate ( $\text{HCO}_3^-$ ) and hydrogen ions ( $\text{H}^+$ ). Increased  $\text{H}^+$  means increased acidity (lower pH). The ocean's acidity increase is already measurable (see Figure 9) as oceans take up  $\text{CO}_2$ . The rate of acidification is limited by the presence of

the carbonate ion ( $\text{CO}_3^{2-}$ ), which binds up most of the newly formed  $\text{H}^+$ , forming bicarbonate. Yet, that buffering reaction consumes carbonate ( $\text{CO}_3^{2-}$ ), reducing the chemical capacity of the near-surface ocean to take up more  $\text{CO}_2$ . Currently, that capacity is only 70% of what it was at the beginning of the industrial era, and at current  $\text{CO}_2$  emissions and resulting further acidification it may well be reduced to only 20% by the end of the twenty-first century. The current rate of ocean acidification appears unprecedented at least over the last 300 million years, based on proxy-data from paleo archives. Acidification will continue to accelerate at least until mid-century, based on projections from Earth system models. Acidification rates are slightly affected by climate change and resulting changes in for example sea surface temperatures, but those effects amount to less than 10% of the changes due to increasing  $\text{CO}_2$ . However, freshening from enhanced ice melt in the Arctic, can significantly accelerate acidification rates.

#### 2.4 Factors driving natural variability of greenhouse gases

In 2015, Earth experienced the start of a strong El Niño event. El Niño events are natural fluctuations

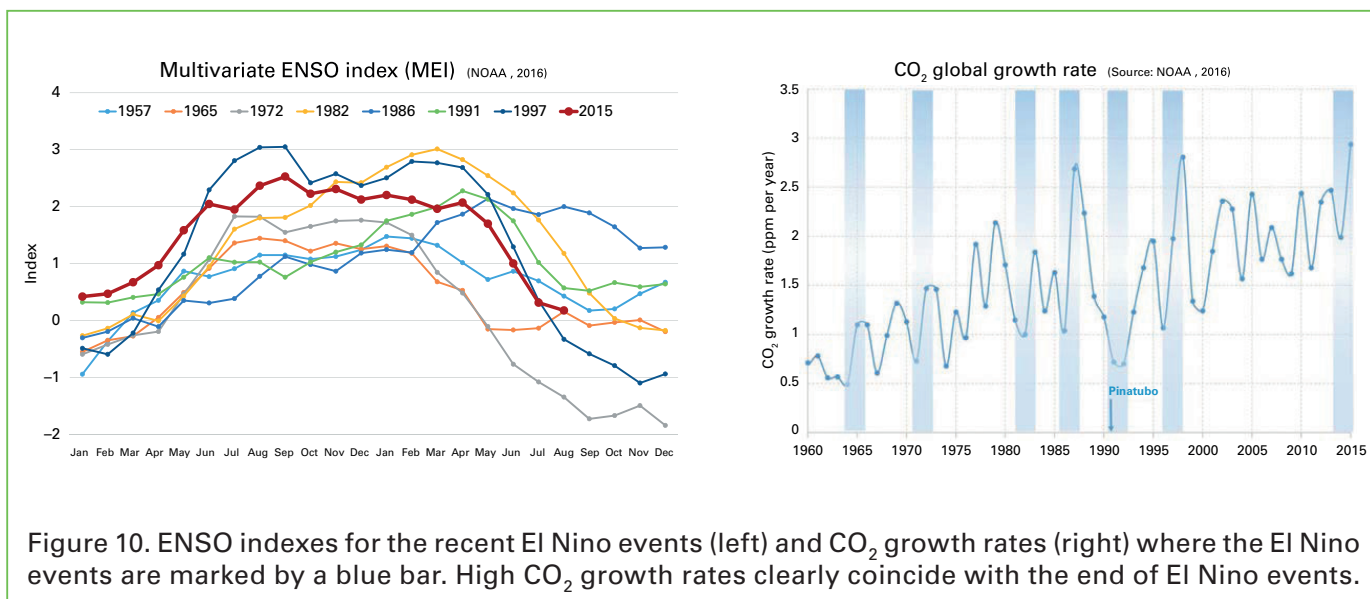


Figure 10. ENSO indexes for the recent El Niño events (left) and CO<sub>2</sub> growth rates (right) where the El Niño events are marked by a blue bar. High CO<sub>2</sub> growth rates clearly coincide with the end of El Niño events.

of the climate system where unusually warm water accumulates in the equatorial Pacific Ocean. El Niño events are associated with abnormal weather patterns such as strong storms in some places and droughts or flooding in others. A typical El Niño event lasts 9 months to 2 years. This phenomenon is witnessed roughly every 2–7 years, although this time the previous large El Niño appeared 18 years ago.

The left curve in Figure 10 shows the multivariate El Niño/Southern Oscillation (ENSO) index that indicates the strength of the El Niño events. ~~The largest El Niño events since 1950 are shown.~~ The 2015/16 El Niño was one of the eight strongest since 1950 and was associated with 16 consecutive months of record global temperatures. With the exception of the years following the eruption of Mt Pinatubo in 1991, we also witness increased growth rates of atmospheric carbon dioxide (CO<sub>2</sub>) following El Niño events (right curve in Figure 10). The plot is based on the CO<sub>2</sub> global growth rate as estimated from NOAA global in situ network with data starting in 1960. The periods with seven largest El Niño events since 1960 are highlighted in blue.

Despite the increasing emissions from ~~fossil fuel energy,~~ ocean and land biosphere still take up about half of the anthropogenic emissions as described above. There is, however, potential that these sinks might become saturated, which will increase the fraction of emitted CO<sub>2</sub> that stays in the atmosphere and thus may accelerate the CO<sub>2</sub>

atmospheric growth rate. During El Niño events, the uptake by land is usually decreased. As during the previous significant El Niño of 1997/1998, the increase in net emissions is likely due to increased drought in tropical regions, leading to less carbon uptake by vegetation and increased CO<sub>2</sub> emissions from fires. According to the Global Fire Emission Database, CO<sub>2</sub> emissions in equatorial Asia were 0.34 Gt C in 2015 (average for the period 1997–2015 is 0.15 Gt C). Other potential feedback can be expected from changes other than El Niño itself, because of atmospheric circulation changes due to large-scale sea-ice loss in the Arctic, increase in inland droughts due to warming, permafrost melting and changes in the thermohaline ocean circulation of which El Niño is in fact a minor modulator.

### 3. Putting current CO<sub>2</sub> levels into historic perspective

#### 3.1 Recent changes in CO<sub>2</sub> in comparison to inter-glacial variations

23,000 years ago, Earth emerged from the last ice age as atmospheric CO<sub>2</sub> concentrations and temperature began to rise. Between 23,000 and 9,000 years ago, the amount of CO<sub>2</sub> in the Earth’s atmosphere increased by 80 ppm, rising from 180 to 260 ppm. State of the art measurements and analytical techniques show that during this particular transition from the ice age to the interglacial period the increases in CO<sub>2</sub> occurred several centuries before the associated

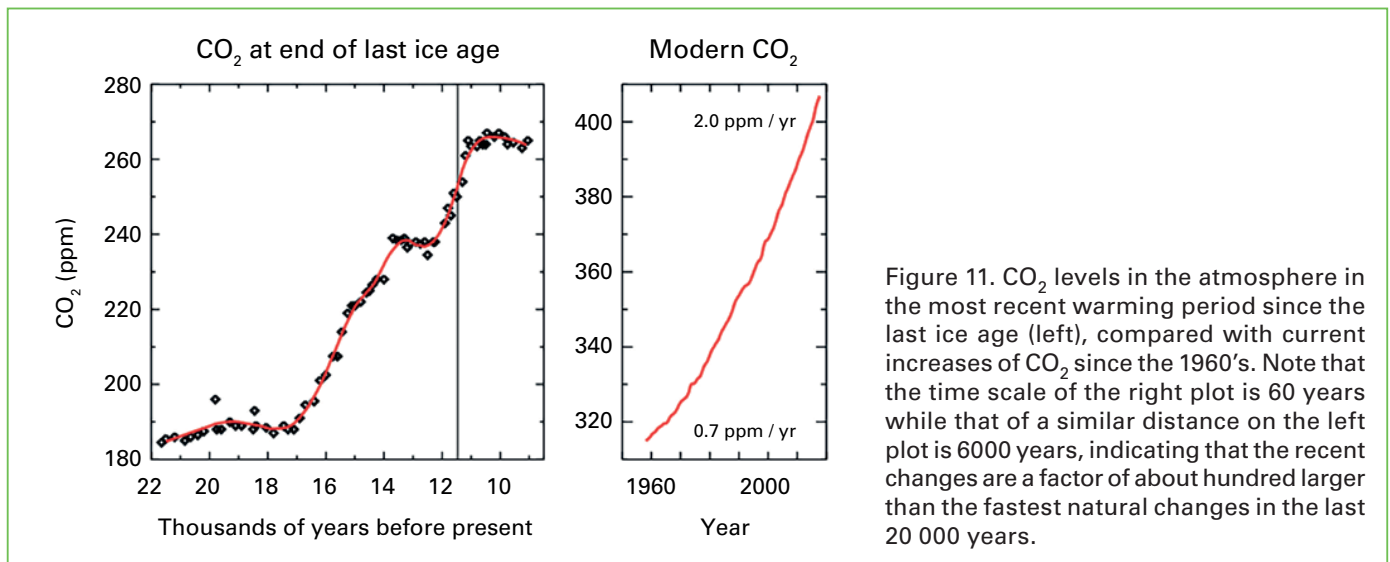


Figure 11. CO<sub>2</sub> levels in the atmosphere in the most recent warming period since the last ice age (left), compared with current increases of CO<sub>2</sub> since the 1960's. Note that the time scale of the right plot is 60 years while that of a similar distance on the left plot is 6000 years, indicating that the recent changes are a factor of about hundred larger than the fastest natural changes in the last 20 000 years.

temperature changes. The West Antarctica ice core record reveals three distinct types of CO<sub>2</sub> variability during this time period (Figure 11).

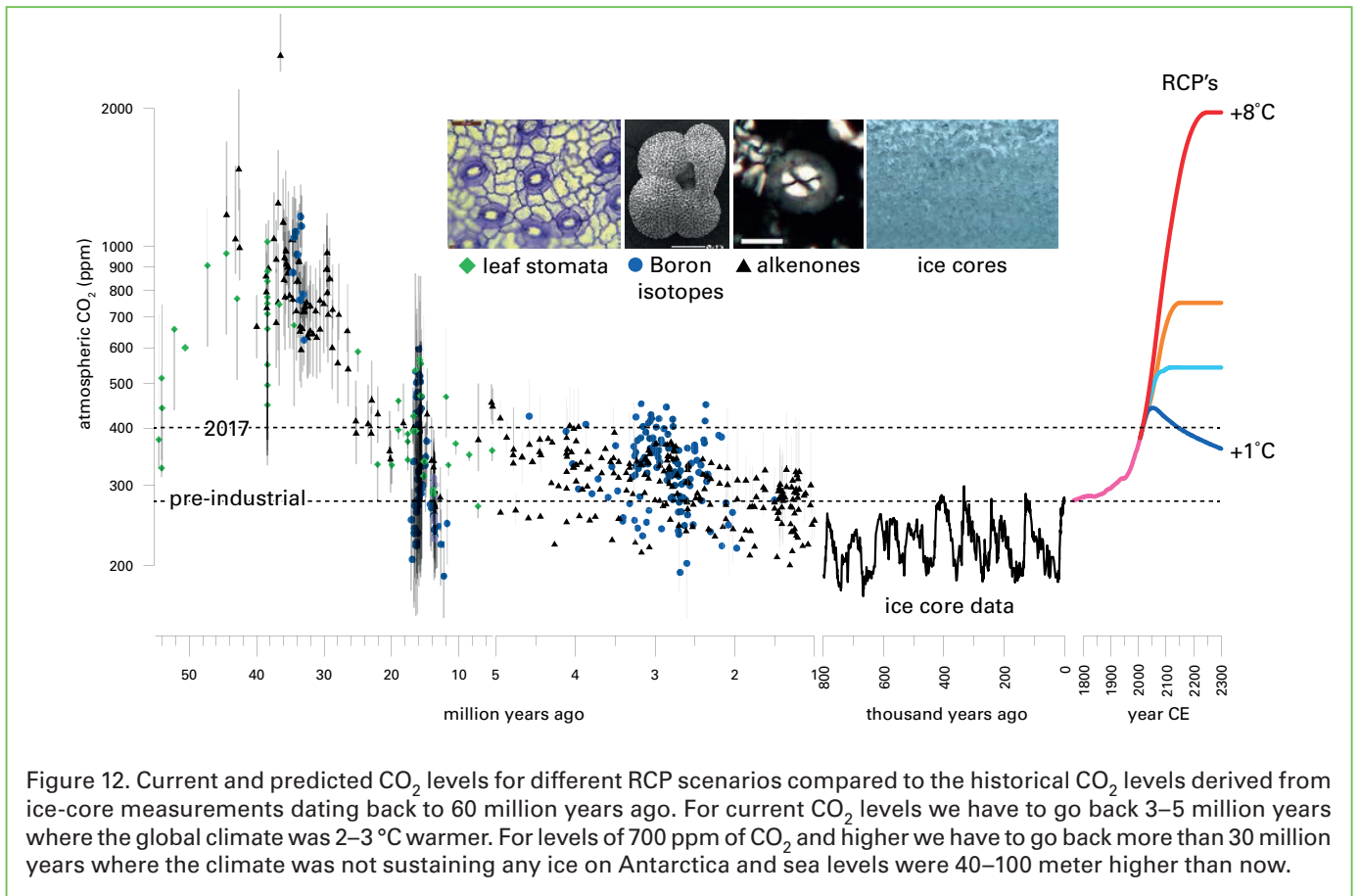
**Slow CO<sub>2</sub> increases:** CO<sub>2</sub> increased slowly at about 10 ppm per 1,000 years between 18,000 and at 13,000 years ago. This slow change is thought to be due to the enhanced release and reduced uptake of carbon stored in the deep ocean, caused by changes in ocean temperature and salinity, a reduction in sea ice and biological activity in the Southern Ocean.

**Abrupt CO<sub>2</sub> increases:** Fast CO<sub>2</sub> increases of 10–15 ppm over 100–200 years are seen at three time periods, 16,000, 15,000 and 12,000 years ago. These three periods of rapid change account for almost half of the total CO<sub>2</sub> increase during the deglaciation and are linked to sudden changes in ocean circulation patterns, a see-saw tug of war between the North Atlantic and Southern Ocean deep ocean currents, causing a rapid release of carbon to the atmosphere. In comparison, fossil fuel combustion caused CO<sub>2</sub> to increase by 120 ppm in the last 150 years, and more than 20 ppm increase during just the last decade.

**Stable CO<sub>2</sub> plateaus:** Curiously, each of the rapid events is followed by stable CO<sub>2</sub> conditions that last about 1,000–1,500 years. While the explanation for these stable conditions is still debated, plausible causes are further changes in ocean circulation from the melting ice sheets, slow changes in growth of land plants and ocean-atmosphere exchange following the rapid CO<sub>2</sub> increase.

### 3.2 Current CO<sub>2</sub> levels in the perspective of paleo climate

Geological records that pre-date ice core archives provide an opportunity to learn how our Earth system responded when atmospheric carbon dioxide concentrations were least similar to those recorded today and expected in the coming decades (Figure 12). Information derived from alkenones, boron isotopes and fossil leaf stomata preserved in layers of rock and sediment provide estimates of CO<sub>2</sub> concentrations over the past many millions of years. These data help us estimate the sensitivity of the Earth's environmental systems to CO<sub>2</sub> concentrations that were higher than pre-industrial levels and thus help to test and improve climate, ice sheet, and Earth system models. Time periods of interest include the mid-Pliocene, 3–5 million years ago, the last time Earth's atmosphere contained 400 ppm CO<sub>2</sub>. Global mean surface temperatures were 2–3 °C warmer than today, ice sheets in Greenland and West Antarctica melted and even parts of East Antarctica's ice had retreated causing sea level to rise 10–20 m higher than today. During the mid-Miocene, some 15 to 17 million years ago, atmospheric CO<sub>2</sub> reached 400–650 ppm and global mean surface temperatures were 3 to 4 °C warmer than today. During the warmest intervals, East Antarctica's ice sheets retreated to the continent's interior causing sea level to rise up to 40 m. Prior to 34 million years ago, atmospheric CO<sub>2</sub> levels were typically >1,000 ppm. Temperatures were so warm that ice sheets were unable to grow in Antarctica.

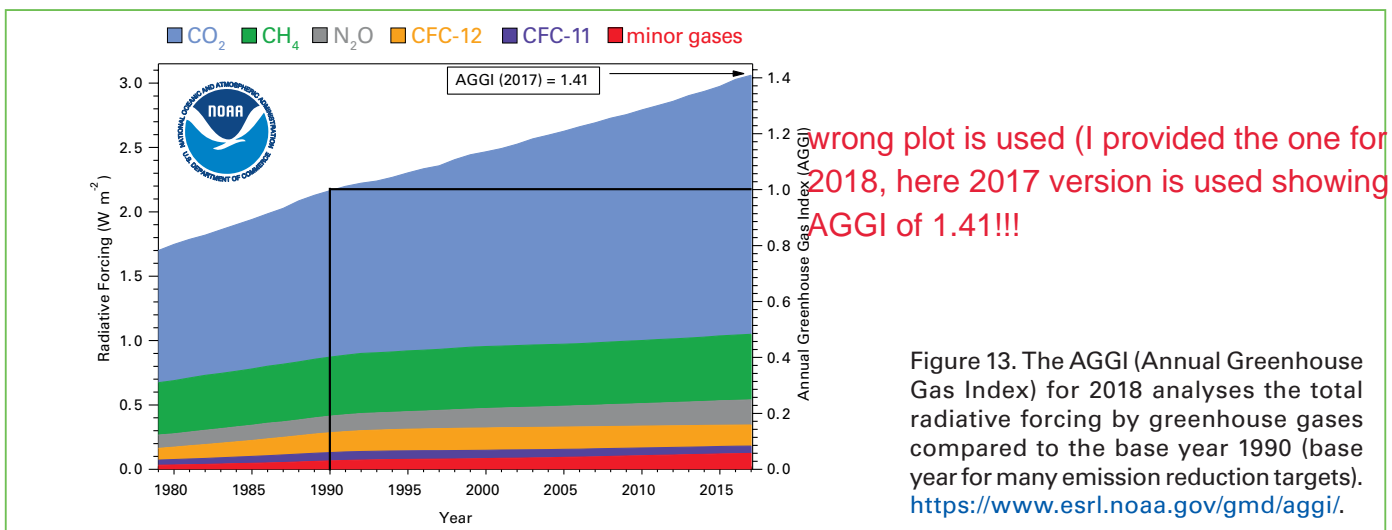


#### 4. The impact of greenhouse gases on climate

The impact of greenhouse gases on climate is expressed in the terms of radiative forcing (the additional energy available in the atmosphere due to the presence of greenhouse gases and the other radiative active agents).

The NOAA Annual Greenhouse Gas Index (Figure 13) shows that from 1990 to 2018 radiative forcing by long-lived greenhouse gases (LLGHGs) increased by 43%, with CO<sub>2</sub> attributing to about 82% of this increase.

The suite of the long-lived greenhouse gases includes sulphur hexafluoride (SF<sub>6</sub>),



## chlorofluorocarbons

ozone-depleting CFCs and minor halogenated gases.  $\text{SF}_6$  is a potent long-lived greenhouse gas. It is produced by the chemical industry, mainly as an electrical insulator in power distribution equipment. Its current mole fraction is more than twice the level observed in the mid-1990s. The stratospheric ozone-depleting CFCs, together with minor halogenated gases, contribute approximately 11% of the radiative forcing by long lived greenhouse gases. While CFCs and most halons are decreasing, some hydrochlorofluorocarbons (HCFCs) and hydrofluorocarbons (HFCs), which are also potent GHGs, are increasing at relatively rapid rates, although they are still low in abundance (at ppt levels) as presented in Figure 14.

### 5. Use of atmospheric observations to improve the knowledge of emissions

The Montreal Protocol on Substances that Deplete the Ozone Layer was designed to protect the stratospheric ozone layer by restricting the production of ozone depleting substances (ODSs) like chlorofluorocarbons (CFCs). Since it entered into force in January, 1989, the Protocol and its subsequent revisions have resulted in reductions of known production and consumption of chlorofluorocarbons and other ozone depleting substances, and in reductions in the emissions of these compounds to the atmosphere that have been verified through atmospheric measurements

and modelling. CFC-11 (trichlorofluoromethane, or  $\text{CCl}_3\text{F}$ ) production reported under the Montreal Protocol declined to zero by 2010. As CFC-11 was phased out, its atmospheric abundance peaked in the early 1990s and then declined, largely consistent with declining production and residual emissions from CFC-11 stored in existing products and equipment ("banks") which gradually escapes.

Atmospheric measurements of CFC-11 made by independent global networks show that since 2012 the rate of decrease in atmospheric CFC-11 has slowed to roughly two thirds of the rate that was observed between 2002 and 2012. These global trends are shown in the Figure 15 on the left for the AGAGE (Advanced Global Atmospheric Gases Experiment; black) and NOAA (National Oceanic and Atmospheric Administration; red) independent measurement networks. Also shown in the inset is the trend that was predicted in 2014 by the WMO (blue dashed) assuming adherence to the Montreal Protocol.

Modelling results lead to the robust conclusion that these changes are predominately related to increased CFC-11 emissions rather than to other possible causes such as changing atmospheric transport. This conclusion is supported by recent increases in the Northern Hemisphere to Southern Hemisphere difference. Correlations between elevated abundances of CFC-11 and other measured

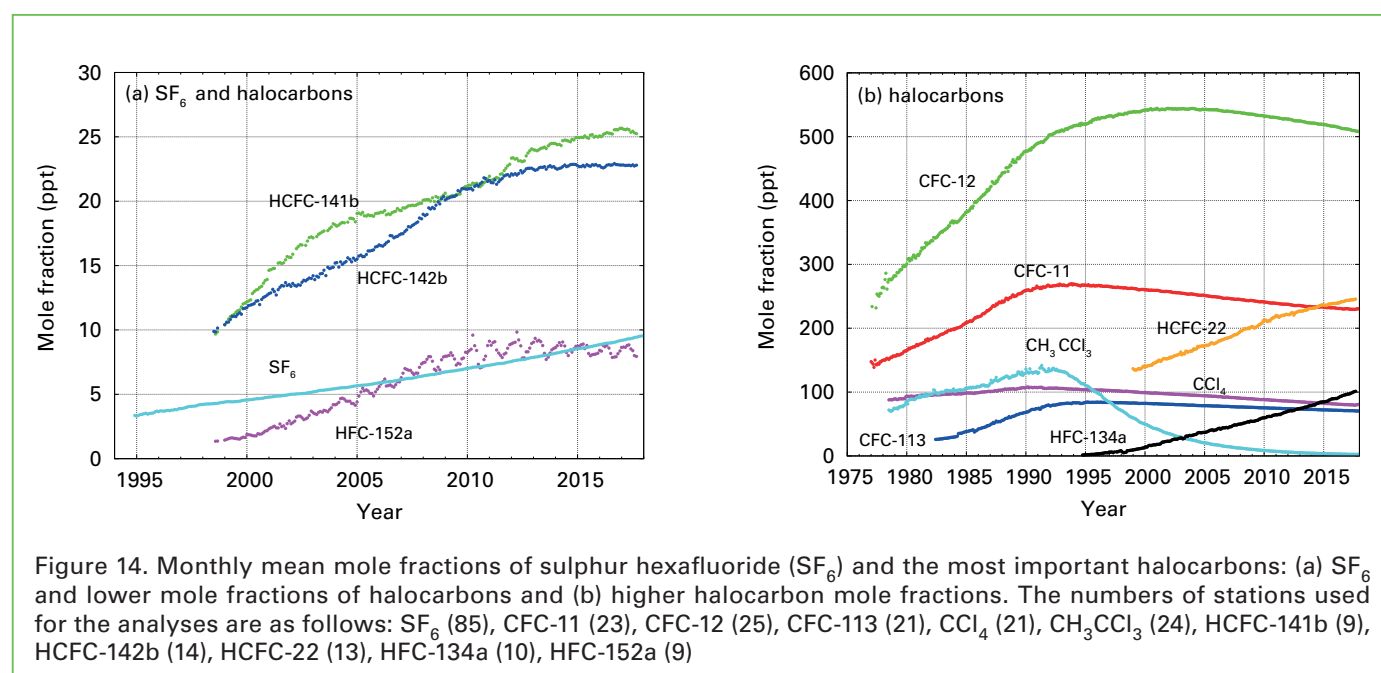


Figure 14. Monthly mean mole fractions of sulphur hexafluoride ( $\text{SF}_6$ ) and the most important halocarbons: (a)  $\text{SF}_6$  and lower mole fractions of halocarbons and (b) higher halocarbon mole fractions. The numbers of stations used for the analyses are as follows:  $\text{SF}_6$  (85), CFC-11 (23), CFC-12 (25), CFC-113 (21),  $\text{CCl}_4$  (21),  $\text{CH}_3\text{CCl}_3$  (24), HCFC-141b (9), HCFC-142b (14), HCFC-22 (13), HFC-134a (10), HFC-152a (9)

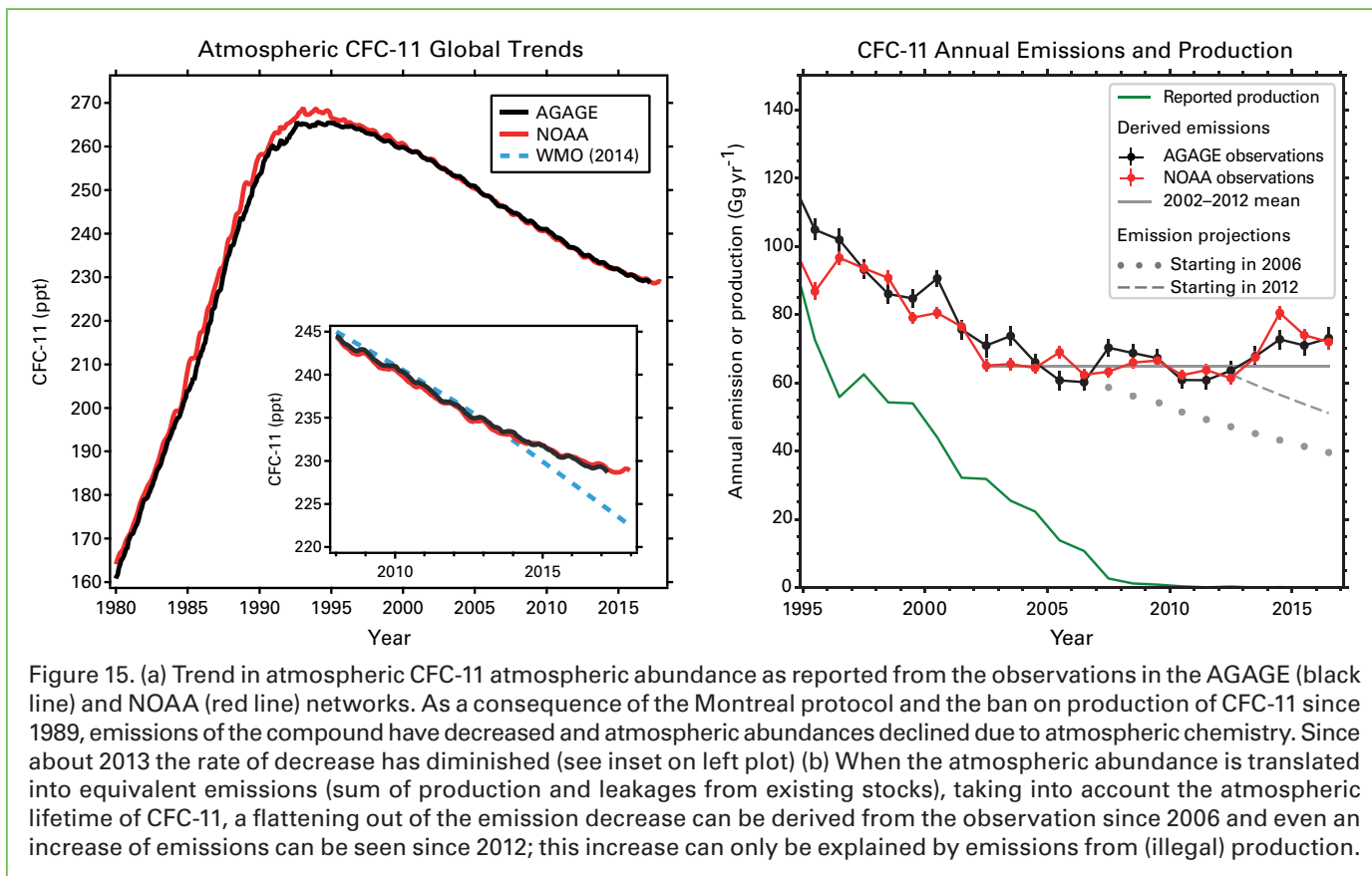


Figure 15. (a) Trend in atmospheric CFC-11 atmospheric abundance as reported from the observations in the AGAGE (black line) and NOAA (red line) networks. As a consequence of the Montreal protocol and the ban on production of CFC-11 since 1989, emissions of the compound have decreased and atmospheric abundances declined due to atmospheric chemistry. Since about 2013 the rate of decrease has diminished (see inset on left plot) (b) When the atmospheric abundance is translated into equivalent emissions (sum of production and leakages from existing stocks), taking into account the atmospheric lifetime of CFC-11, a flattening out of the emission decrease can be derived from the observation since 2006 and even an increase of emissions can be seen since 2012; this increase can only be explained by emissions from (illegal) production.

gases further suggest that these increases originate from emissions in eastern Asia.

Separate CFC-11 emission trends resulting from model calculations based on data from each of the global measurement networks AGAGE (black) and NOAA (red) are shown in the Figure 15 on the right from the 2018 WMO Ozone Assessment. They are contrasted to the CFC-11 production as reported under the Montreal Protocol (green). These results show a levelling off of CFC-11 emissions around 2005, followed by an emission increase of about 15% after 2012. Emissions scenario projections for the years 2006 and 2012 based on atmospheric data, reported production, and releases from banks are shown as dots and dashes (grey), respectively. There are indications that the increases in CFC-11 emissions have been driven, at least in part, by an increased demand for foam insulation used in buildings to improve

energy efficiency and hence to reduce carbon dioxide emissions from the burning of fossil fuels.

Recognizing the value that atmospheric observations can bring in improving the knowledge of the greenhouse gas distribution and trends on national and sub-national scale, WMO established an Integrated Global Greenhouse Gas Information System (IG<sup>3</sup>IS). IG<sup>3</sup>IS serves as an international coordination framework for the development and utilization of harmonized methods for emission estimates based on atmospheric observations. IG<sup>3</sup>IS was mentioned as a framework to improve estimates of GHG concentrations and fluxes by the 50th session of the Subsidiary Body for Scientific and Technological Advice (SBSTA), and in the 2019 Refinement to the 2006 Guidelines for National Greenhouse Gas Inventories adopted and accepted during the 49th Session of the IPCC in May 2019 (Volume I, Chapter 6).